

Liquid-gas separation in colloidal electrolytes

José B. Caballero,¹ Antonio M. Puertas,^{1,*} Antonio Fernández-Barbero,¹
F. Javier de las Nieves,¹ J.M. Romero-Enrique,² and L.F. Rull²

¹Group of Complex Fluids Physics, Department of Applied Physics, University of Almería, 04120 Almería, Spain

²Depto. de Física Atómica, Molecular y Nuclear, Área de Física Teórica,
Universidad de Sevilla, Aptdo. 1065, 41080 Sevilla, Spain

(Dated: May 24, 2019)

The liquid-gas transition of an electroneutral mixture of oppositely charged colloids, studied by Monte Carlo simulations, is found in the low temperature – low density region. The critical temperature shows a non-monotonous behavior as a function of the interaction range, κ^{-1} , with 3D-Ising criticality at all κ around the peak. An island of coexistence is thus predicted in the κ - ρ plane. The system is arranged in such a way that each particle is surrounded by shells of particles with alternating charge and both neutral and charged clusters are obtained in the vapor phase.

PACS numbers: 82.70.Dd, 82.70.Gg, 64.70.Pf

Electrostatic correlations play an important role in model, biological and applied systems¹, being their comprehension a huge challenge for the liquid state researchers. While progress has been made in understanding the influence of those correlations in simpler ionic systems, only recently the importance of colloid-colloid correlations has been acknowledged. Furthermore, for charged colloidal systems, the interaction depends not only on the charge density and distribution, but also on the solvent properties. The interactions are mediated by the solvent, and thus tunable by acting on it (added salt, temperature...). This is the reason why phase diagrams are in general richer in colloidal systems².

The Restricted Primitive Model (RPM) for ionic fluids is the simplest mixture showing strong effects due to charge correlations³. This model undergoes a liquid-gas transition at low temperature and density due to the strength of the correlations^{1,4} with Ising-like behavior⁵, despite the long range of the interactions. This model has been also extended to tackle size or charge asymmetries and applied to dipolar systems⁶, showing a vapor-liquid coexistence island.

In this letter, we study the liquid-gas transition in the colloidal analogue of the RPM, using a mixture of oppositely charged colloids by means of computer simulations. We pay especial attention to the range of the electrical interaction among particles, experimentally controlled by the electrolyte concentration in the medium. We find an unexpected non-monotonous behavior for the critical temperature with the range of interaction, thus showing a re-entrance phenomenon (fluid – phase separation – fluid) by increasing the salt concentration. This is a collective effect since a third term in the virial expansion of the pressure is necessary to describe the non-monotonous critical temperature curve. This fact is then rationalized from the strong correlation between oppositely charged particles, leading in both phases to particles surrounded by shells of alternating charges and clusters growing in the dilute phase. Under this configuration, repulsive and attractive interactions are screened in a different way, provoking a maximum in the critical temperature. Fi-

nally, we show that an increase of the amount of clusters is not a signature of the proximity to the phase transition. That is actually driven by the energy gain in the dense phase to overcome the entropy lost in forming a liquid.

We simulate a 1:1 binary mixture of N spherical colloidal particles, $N/2$ bearing a surface potential $+\phi$ and $N/2$ with $-\phi$. The interaction between colloids is modeled by the effective DLVO electrostatic interaction⁷, plus a hard-core repulsion,

$$V(r_{ij}) = V_{HS}(r_{ij}) + \phi_i \phi_j \exp\{-\kappa(r_{ij} - \sigma)\} \quad (1)$$

where V_{HS} is the hard-sphere potential for a particle of diameter σ , ϕ_i and ϕ_j are the surface potentials of the interacting particles (in appropriate units) and κ is the inverse Debye length. Hereafter, we use reduced units: $\sigma = 1$, $U^* = U/\phi^2$, $T^* = k_B T/\phi^2$ and the density $\rho^* = N\sigma^3/V$, where N is the number of particles, and V the volume of the system.

The liquid-gas transition, studied by means of Gibbs Ensemble Monte Carlo (GEMC) and Grand Canonical (GC) simulations⁸, is found in the low- T -low- ρ region, where strong correlations between oppositely charged particles emerge, producing a thermodynamic instability^{1,9}. We find liquids and vapours composed of the same number of positive and negative particles on average. The GEMC results for different κ are presented in Fig. 1. In contrast to monocomponent attractive systems¹¹, the critical temperature evolves non-monotonically. At low κ , demixing occurs at higher temperatures the shorter the interaction range, and only at high κ , the critical temperature moves to lower values as κ increases. Noteworthy, this behavior implies a closed region of phase separation in the constant- T , κ - ρ plane, which is experimentally more accessible than the T - ρ one for colloids. A reentrance phenomenon is thus predicted by increasing the salt concentration, from fluid to phase separation and to fluid again. Note that not only the position of the phase boundary changes but also its shape

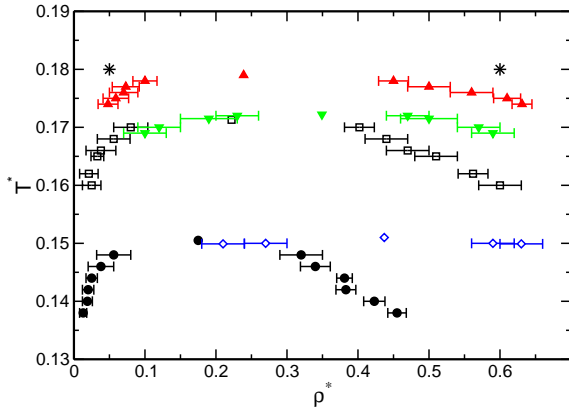


FIG. 1: Gas-liquid coexistence points for different values of κ : $\kappa = 3.9$ circles, $\kappa = 6$, open squares, $\kappa = 10$, upward triangles, $\kappa = 15$, downward triangles, and $\kappa = 20$, diamonds. The points without error bars mark the critical points.

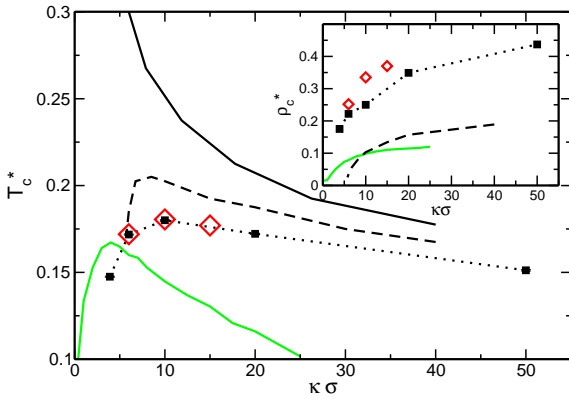


FIG. 2: Critical temperature and density (inset) as a function of $\kappa\sigma$: fill squares from GEMC and empty red diamonds from Grand Canonical simulations. Black lines are the results using the virial expansion for the pressure up to second (solid line) and third order (broken line) in density. Green lines are results from MSA on a Yukawa mixture¹⁶.

depends on $\kappa\sigma$, asymmetric at low $\kappa\sigma$ and symmetric at high ones. Interestingly, the liquid-gas transition in the RPM is also highly asymmetric^{12,13}, whereas the boundary in a monocomponent attractive fluid is symmetric.

The critical temperature and density from both GEMC and GC simulations are presented in Fig. 2 as a function of κ . The agreement between both simulation results confirms the behavior described above, although the critical density is better estimated with the GC simulations. The critical parameters have been calculated using the virial expansion of the pressure up to second and third orders (continuous and dashed lines in Fig. 2, respectively): $\beta P(\rho) = \beta P_{HS}^{CS}(\rho) + B_2\rho^2 + B_3\rho^3$, where $P_{HS}^{CS}(\rho)$ is the Carnahan-Starling expression for the pressure of hard spheres^{14,15}. The second order expansion produces a liquid-gas transition, driven by the attractions between oppositely charged particles, which behaves monotonically with $\kappa\sigma$. On the other hand, the expansion up to

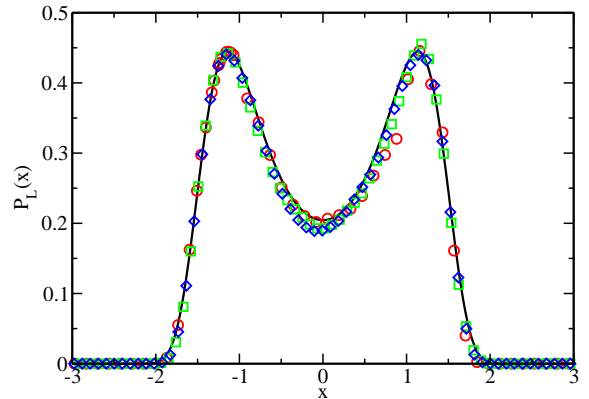


FIG. 3: Order parameter probability distribution $P_L(x)$ for $L=10$ and different range of interaction: $\kappa\sigma = 6$ (red circles), $\kappa\sigma = 10$ (green squares) and $\kappa\sigma = 15$ (blue diamonds); solid line for 3D-Ising model.

third order correctly reproduces the maximum in T_c vs. $\kappa\sigma$. Because B_3 is needed to reproduce qualitatively the results, the increasing trend of T_c vs. $\kappa\sigma$ at long interaction ranges comes from the interaction between, at least, three particles, mainly the repulsion between two particles with similar charge attracted to a third one. This repulsion is more important for lower κ , whereas the attraction energy is not greatly increased. These results also agree qualitatively with previous calculations for an attractive-repulsive mixture of Yukawa potentials using an expansion of the internal energy and the equation of state, based on the mean-spherical approximation (MSA)¹⁶.

GC simulations also allow to study the criticality using the mixed field scaling method by Bruce and Wilding¹⁰. Fig. 3 shows the marginal distribution functions for $\kappa\sigma = 6, 10$ and 15 of a scaling variable $x \propto \delta M$. The magnetization-like operator $M \propto \rho + su$, is a linear combination of density and energy and $\delta M = M - \langle M \rangle$ the deviations from its mean value. The scaling of the proportionality constants of x with the box size L , allows calculation of the critical exponent ratio β/ν . The value obtained is similar to that of the Ising model ($\beta/\nu = 0.518$) for the three ranges studied: $\beta/\nu = 0.523(14), 0.509(23)$ and $0.503(20)$ for $\kappa\sigma = 6, 10$ and 15 , respectively. The overlapping between data and the 3D-Ising curve (solid line) in Fig. 3 and the similar numerical values for the ratios β/ν , support the compatibility with 3D-Ising criticality, as expected for short-range potentials.

As in the ionic fluids, the demixing in a dense and a dilute phase is driven by the strong correlations between oppositely charged particles^{1,9}. We have investigated the internal correlations in two supercritical ($T^* = 0.18$) states, $\rho^* = 0.6$ and $\rho^* = 0.05$, marked in Fig. 1 as asterisks. Fig. 4 plots the opposite sign, $g_{+-}(r)$, and same sign (inset), $g_{++}(r) = g_{--}(r)$, contributions to the pair distribution function for the dense state (with $\kappa\sigma = 2, 6$ and 15). The system is composed of layers with alternat-

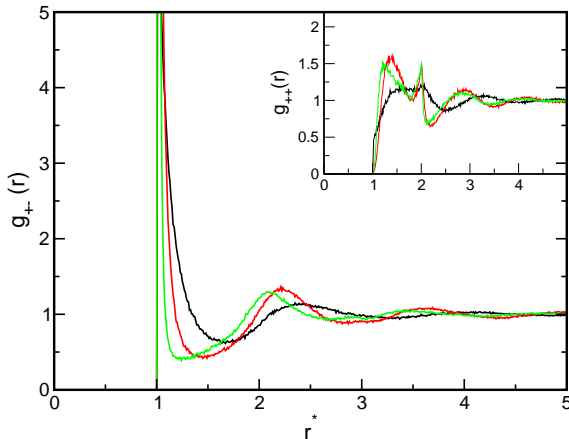


FIG. 4: Partial pair distribution functions for $T = 0.18$ and $\rho = 0.6$ with $\kappa = 2$ (black curve), $\kappa = 6$ (red curve) and $\kappa = 15$ (green curve); opposite sign (main figure) and same sign (inset).

ing sign particles surrounding every particle; first layer of particles of opposite sign, second one of the same sign... This structure extends to distances of several radii, much larger than the interaction range. As observed in the Figure, the peaks shift to shorter distances as κ increases. Similar features have been predicted using the MSA for the partial structure factors¹⁷.

Second neighbors of one particle comprise the first shell of particles with the same sign, which moves to larger distances as κ decreases. This is due to the repulsion between similarly charged particles and correlations through unlike particles. The first neighbor layer, thus, drive the gas liquid transition, whereas the second one impedes it, resulting in a maximum of the critical temperature. A peak at $r = 2\sigma$ marks the presence of linear arrangements (three particles long) at all ranges studied. This peak is not caused by the repulsion of the central particle (because the repulsion range is too short), but due to the repulsion of the particles in the second layer, first peak in $g_{++}(r)$. Visual inspection of the system shows that these strings are distributed randomly (thus cannot be attributed to crystallites), and are only three particles long (no peak at $r = 3\sigma$ in $g(r)$).

Now we move to the dilute supercritical state $T = 0.18$ and $\rho = 0.05$, presented in Fig. 5 for different interaction ranges (upper panel). The system is composed of clusters of particles⁹, and the fraction of particles in every cluster, x_n , is presented in the lower panel of the figure for different values of κ . Again the layering of particles inside clusters is observed although only two or three layers are seen due to the finite size of the clusters. The layers move closer as κ increases, the effect being more dramatic than in the dense state due to the lower density of the system. Notably, the absence of the peak at $r = 2\sigma$, confirms the collective origin of the linear structures found in the dense phase (Fig. 4).

Different from the RPM^{18,19}, the distribution of clus-

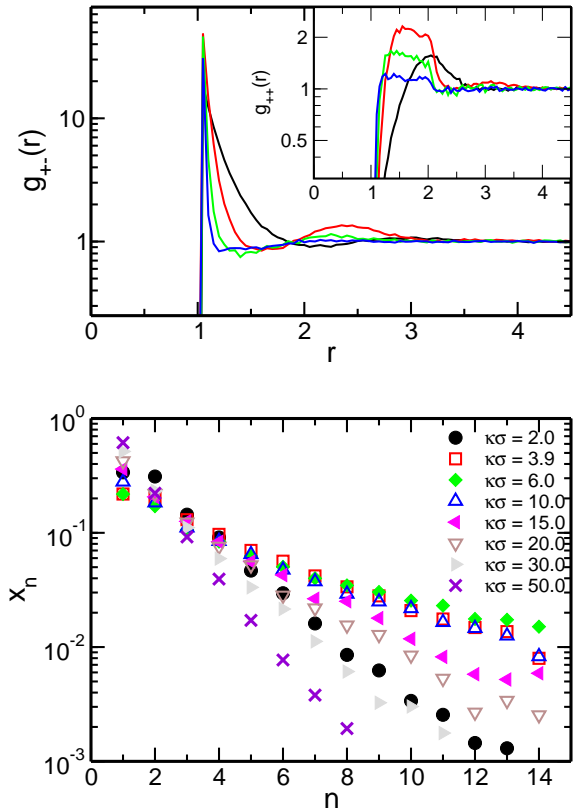


FIG. 5: Upper panel: Partial pair distribution functions for $T^* = 0.18$ and $\rho = 0.05$ with $\kappa = 2$ (black curve), $\kappa = 6$ (red curve), $\kappa = 15$ (green curve) and $\kappa = 30$ (blue curve); oppositely sign (main figure) and same sign (inset). Lower panel: Fraction of particles in a cluster with n particles for the same state and different κ , as labeled. x_n is normalized as: $\sum x_n = 1$.

ters is monotonous, containing both neutral and charged clusters, no matter how close to the transition. However, this distribution shows also a non-monotonic behavior with κ ; for long ranges the number of large clusters increases when κ increases, whereas the opposite trend is observed at high κ , the maximum number of big clusters found for $\kappa\sigma = 6.0$ (for not-too-big clusters, the maximum is at $\kappa\sigma = 3.9$). These values do not agree with the maximum of T_c^* , which indicates that maximal proximity to the transition does not imply maximal tendency to form large clusters in dilute systems.

Finally, to complete the understanding of the phase transition and its driving mechanism, Fig. 6 depicts the internal (electrostatic) energy with its contributions from attractions and repulsions. The same supercritical states are presented ($T^* = 0.18$; $\rho^* = 0.6$ (upper panel) and $\rho^* = 0.05$ (lower panel)). At low κ , the total energy comprises repulsive and attractive contributions. For larger κ , however, the energy contains only the attractive contributions due to the different distances between similar sign and opposite sign pairs (see Fig. 4). Therefore, the behavior at high κ is similar to that of a monocompo-

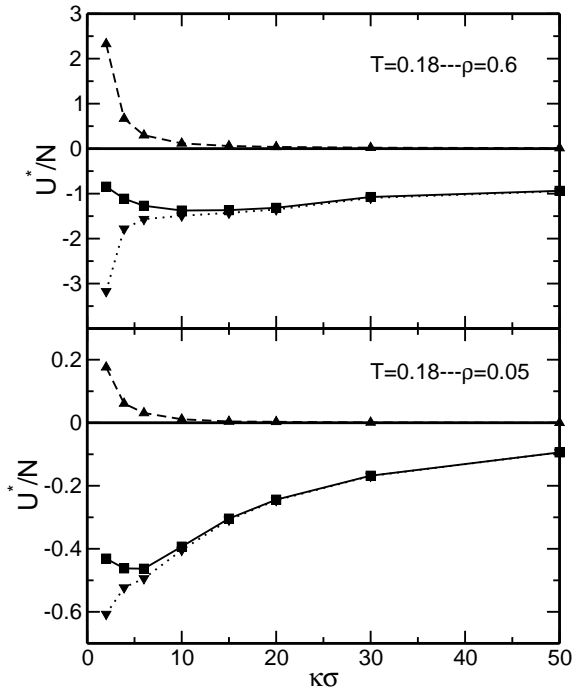


FIG. 6: Electrostatic energy (squares), and contributions from repulsions (upwards triangles) and attractions (downwards triangles) for two states as labeled.

ment system. For the dilute state, the clustering implies a low number of bonds, as compared to the dense state, resulting in a lower energy (in absolute value). The minimum in the energy can be rationalized using simple small clusters, i.e. trimers and tetramers²⁰.

Comparison of the energy curves with the behavior of

critical temperature shows that the driving mechanism for liquid-gas separation in this system is the energy gain in forming a dense (liquid) phase, and not the ability to form large clusters in dilute phases (see Fig. 6), as proposed for the asymmetric ionic fluids²¹. The effect arises from the difference in the number of interacting pairs of similarly charged colloids in the dilute and dense phases. The internal energy calculated using the MSA for a mixture of Yukawa potentials shows similar trends, with minima moving to higher κ as the density increases¹⁶.

In conclusion, we have studied the liquid-gas transition in a system which can be considered as the colloidal analogue of the ionic fluid, i.e. a 1:1 mixture of oppositely charged colloids. The coexistence region is found in the low density-low temperature region, with 3D-Ising criticality. The critical temperature shows a non monotonic behavior with the range of the interaction, κ ; increasing in low values of κ and decreasing for the higher ones. This prediction implies a closed region of liquid-gas demixing at constant temperature in the $\kappa - \rho$ plane. The condensed phases are arranged in such a way that each particle is surrounded by shells of particles with alternating charge. The internal energy shows that the overall trend of the critical temperature is lead by the energy gain in forming a dense phase. Liquid-gas separation at long ranges is hindered by the repulsion between similarly charged particles bonded to a third one (of opposite sign).

J.B.C, A.M.P., A.F.B. and F.J.N. acknowledge the financial support by MCyT, under projects no. MAT 2003-03051-C03-01 and MAT 2004-03581, and J.M.R.E. and L.F.R. under projects no. PB97-0712 and BQU2001-3615-CO2-02.

* Corresponding author: apuertas@ual.es

¹ Y. Levin, Rep. Prog. Phys. **65** 1577 (2002).

² *Observation, Prediction and Simulation of phase transitions in complex fluids* Ed. M. Baus, L.F. Rull, J.-P. Ryck-aert (Kluwert, Dordrecht, 1995).

³ D.A. McQuarrie, *Statistical Mechanics* (Harper & Row, New York, 1976).

⁴ J.M. Romero-Enrique, L.F. Rull, A.Z. Panagiotopoulos, Phys. Rev. E **66** 041204 (2002).

⁵ Y.C. Kim, M.E. Fisher, E. Luijten, Phys. Rev. Lett. **91** 065701 (2003).

⁶ S. McGrother, G. Jackson, Phys. Rev. Lett. **76** 4183 (1996).

⁷ E.J.W. Verwey, J.T.G. Overbeek, *Theory of the Stability of Lyophobic Colloids* (Elsevier, Amsterdam, 1948).

⁸ Multiparticle moves do not increase the equilibration rate, due to the large density of the saturated liquid, as compared with RPM one. Further technical details of the GEMC simulations can be found in Ref.⁹. GC simulations with box size $L = 8, 9, 10$ and 12 were run to analyse of the critical behaviour.

⁹ J.B. Caballero, A.M. Puertas, A. Fernández-Barbero, F.J.

de las Nieves, J. Chem. Phys. **121**, 2428 (2004).

¹⁰ A.D. Bruce, N.B. Wilding, Phys. Rev. Lett. **68** 193 (1992).

¹¹ W. Poon, P.N. Pusey, H.N.W. Lekkerkerker, Phys. World April 1996 pg. 27.

¹² G. Orkoulas, A.Z. Panagiotopoulos, J. Chem. Phys. **110** 1581 (1998).

¹³ J.M. Caillol, D. Levesque, J. J. Weis, J. Chem. Phys. **107** 1565 (1997).

¹⁴ J.P. Hansen, I.R. McDonald, *Theory of Simple Liquids* Elsevier Academic Press (Amsterdam, 1990).

¹⁵ B_2 and B_3 are calculated by MonteCarlo integration, from their definitions. The full interaction potential is included in the calculation, and the hard sphere contributions are subtracted (included in $P_{HS}^{CS}(\rho)$).

¹⁶ L. Mier-Y-Terán, S.E. Quiñones-Cisneros, I.D. Núñez-Riboni, E. Lemos-Fuentes, Molec. Phys. **95** 179 (1998).

¹⁷ H. Ruiz-Estrada, I.D. Núñez-Riboni, C. Romero-Salazar, J. Nieto-Frausto, Mol. Phys. **99** 1299 (2001).

¹⁸ F. Bresme, E. Lomba, J.J. Weis, J.L.F. Abascal, Phys. Rev. E **51** 289 (1995).

¹⁹ J.-M. Caillol, J.-J. Weis, J. Chem. Phys. **109** 7610 (1995).

²⁰ J.B. Caballero, A.M. Puertas, A. Fernández-Barbero, F.J.

de las Nieves, Submitted to Coll. Surf. A.
²¹ Q. Yan, J.J. de Pablo, J. Chem. Phys. **114** 1727 (2001).